PHYSICAL REVIEW A **94**, 043830 (2016)

Enhanced nonlinear imaging through scattering media using transmission-matrix-based wave-front shaping

Hilton B. de Aguiar,[1,*] Sylvain Gigan,[2] and Sophie Brasselet[1,†]
[1]*Aix-Marseille Université, CNRS, Centrale Marseille, Institut Fresnel UMR 7249, 13013 Marseille, France*
[2]*Laboratoire Kastler Brossel, ENS-PSL Research University, CNRS, UPMC Sorbonne Universités, Collège de France, 24 rue Lhomond, 75005 Paris, France*

(Received 6 June 2016; revised manuscript received 22 September 2016; published 18 October 2016; publisher error corrected 24 October 2016)

Despite the tremendous progress in wave front shaping for enhancing imaging penetration depths in scattering media, several factors, among which are significantly low signal-to-noise ratios at large depths, prevent feasibility for nonlinear imaging in biological tissues. Here, we propose an alternative to the traditional schemes that use optimization of a nonlinear signal. By exploiting the linear photons instead of nonlinearly generated ones, we show strong enhancements of nonlinear signals of several orders of magnitude, through thicknesses of a few transport mean free paths, which corresponds to millimeters in biological tissues. This is achieved by measuring the *linear broadband* transmission matrix (TM) of the scattering medium, using a spectral bandwidth comparable to the speckle spectral correlation width. We further highlight several advantages of the use of linear TM for prospective nonlinear imaging deep inside scattering media.

DOI: 10.1103/PhysRevA.94.043830

I. INTRODUCTION

Nonlinear microscopy (NLM) is established as a powerful approach for label-free imaging in biological tissues [1,2]. Despite the impact of NLM on many fields, standard nonlinear imaging modalities can only image at shallow depths, typically a few hundreds of micrometers for biological specimens. The penetration depth is essentially limited by optical aberrations and scattering, which degrade the spatial quality of focusing and decrease the spatiotemporal coherence of short pulse excitation fields that are necessary to build up nonlinear processes. In order to increase the penetration depth of nonlinear imaging, adaptive optics has been introduced to compensate for aberrations from biological samples [3]; however, it is still limited to the use of ballistic photons and existing nonlinear signals, which both quickly fade in the case of strong scattering [4–6].

Wave front shaping (WS) can overcome penetration depth limits in highly scattering media, addressing specifically the scattered photons [7]. Despite the random appearance of the outgoing speckle pattern arising from multiple scattering events, it has nevertheless a deterministic relation with the original incoming wave front, revealed in the transmission matrix (TM) of the scattering medium that connects incoming to outgoing fields. By coherently controlling a speckle pattern, one can increase the energy density at targeted positions, resembling a focus that we call "refocus" in what follows to avoid confusion with a focus obtained from ballistic photons. WS has enabled refocusing through [8,9] or inside [10] scattering media, thanks to the manipulation of the wave front phase or amplitude [11,12].

The combination of WS and NLM is, however, so far limited to only a few demonstrations based on nonlinear feedback optimization [13–15]. This type of feedback is attractive since it intrinsically optimizes the spatial and temporal properties of the refocused beam [7,16–18]. However, it suffers a main limitation: nonlinear optimization requires access to nonlinearly generated photons to start with, which typically implies bright nonlinear samples. It therefore suffers from low signal-to-noise conditions and thus slow optimization procedures. Demonstrations using either a nonlinear guide star [13] or an integrated nonlinear signal [15] have nevertheless been successful even though they have led so far to mild nonlinear enhancements η_{NL} (defined as the ratio between the nonlinear signal obtained at the refocus and prior to the optimization procedure). Ideally, η_{NL} should indeed scale as $\mathrm{N}_{\mathrm{SLM}}^{n}$, where $\mathrm{N}_{\mathrm{SLM}}$ is the number of spatial degrees of freedom (SLM stands for spatial light modulator) and n is the order of the nonlinear process. Besides signal-to-noise issues, one of the main reasons for the lower-than-expected nonlinear enhancements originates from the temporal broadening of the pulse propagating through the scattering medium. In essence, the spectral width ($\Delta\lambda$) of the broadband pulse is larger than the speckle spectral correlation width ($\delta\lambda$) of the scattering medium ($\delta\lambda$ is related to the path-length distribution of photons in the medium). In other words, if the spectral bandwidth of the source ($\Delta\lambda$) is much larger than the speckle spectral correlation width ($\delta\lambda$), many spectrally decorrelated modes propagate through the medium and, in the absence of additional control of the spectral degrees of freedom, the resulting refocused pulse will be broadened temporally, resulting in a poor nonlinear generation. Other limitations further hamper the use of nonlinear optimization for imaging. First, nonlinear optimization methods depend on the nonlinear contrast mechanism used: the coherence of the optical process (harmonic generation versus fluorescence) and its order (second- versus third-order nonlinearities) lead to different dependencies of the optimization that make the result dependent on the feedback nature [15]. Second, imaging nonsparse nonlinear samples is delicate because of a strong nonlinear background arising

*h.aguiar@phys.ens.fr
†sophie.brasselet@fresnel.fr

from the volume excited [15,19,20], which may add possible artifacts in the signal optimization procedure. This last point is specifically addressed in Sec. III C.

In this work, we demonstrate that *linear* TM-based WS generates strong nonlinear signals through scattering media, without the need to optimize nonlinear signal. We essentially exploit the fact that $\delta\lambda$ in biological media at 1–2 mm deep (corresponding to a transport mean free path l_t) [21] are comparable to the bandwidth $\Delta\lambda$ of common laser sources used for NLM (about 100 fs pulse length). The paper is organized as follows. For the sake of comparison, we first present results using a nonlinear feedback optimization (Sec. III A). We then show that a linear-feedback-based TM offers faster nonlinear imaging capabilities and higher signal-to-noise conditions (Sec. III B), not only in the regime where the pulse is not lengthened by the medium ($\delta\lambda > \Delta\lambda$), but also in the regime where the pulse is temporally broadened (upon propagation) to a few times its Fourier transform limited duration (here, approximately threefold). We illustrate the potential of this approach by imaging thick biological specimens which generate a strong nonlinear background [second-harmonic generation (SHG) of collagen fibers], in conditions that would fail using nonlinear feedback optimization (Sec. III C). We then conclude in Sec. IV by discussing the applicability of linear TM to nonlinear imaging *inside* a scattering medium, since it is compatible with other linear-based techniques such as acousto-optical interactions [10], digital optical phase conjugation [22,23], and optical coherent tomography [24].

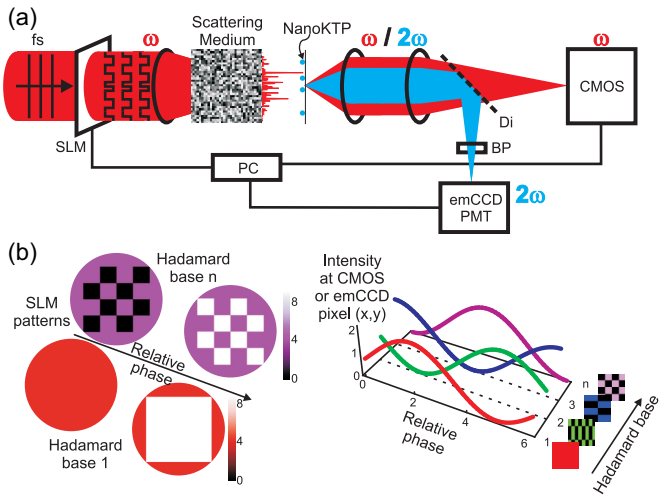

FIG. 1. Wave front shaping experiments for nonlinear microscopy. (a) Simplified experimental layout. The optical wave front is shaped by an SLM and focused inside the scattering medium. The speckle generated outside the scattering medium excites the nonlinear sources (nano-KTP) placed at a plane further imaged on different detectors (emCCD, CMOS, PMT). (b) Methodology used for refocusing using the Hadamard basis. The wave front phase is swept in respect to a reference field (the unmodified periphery outside a Hadamard base), under broadband excitation. At the detectors (a pixel on the emCCD or on the CMOS), a sinusoidal modulation of the intensity is observed, from which each individual phase is stored (per base). After scanning the basis set, the optimal wave front is used for either enhancing the nonlinear signal (emCCD) or linearly refocusing (CMOS) with the nonlinear signal detected in parallel (PMT).

II. EXPERIMENT

A. Optical setup and methodology

Figure 1(a) shows a simplified schematic of the experiment. Short pulses (130 fs, 800 nm, 76 MHz repetition rate, Mira, Coherent) are steered onto a 256 × 256 pixel reflective SLM (Boulder Nonlinear Systems). The SLM is imaged on the back focal plane of the focusing lens [0.32 numerical aperture (NA), achromatic lens, Thorlabs]. The scattering medium is placed between the focusing lens and its focus. The potassium titanyl phosphate nanocrystals (nano-KTP) crystals (150 nm diameter) are deposited on a coverslip (170 μm), and imaged by an objective (40×, 0.75 NA, Nikon) on a 12-bit complementary metal-oxide semiconductor (CMOS) camera (Flea3, Point Grey), and on either an electron multiplying charge-coupled device (emCCD, QuantEM, Roper Scientific) for the nonlinear feedback scheme, or on a large-area photon counting photomultiplier tube (PMT) for the linear feedback scheme (MP 953, PerkinElmer). The nano-KTP sample is typically placed at a millimeter distance (for diffuser), or 100 μm (for TiO_2 films), from the scattering medium. The SHG signal is spectrally separated with a suitable dichroic mirror with 560 nm long-pass (AHF Analysentechnik), short-pass (700 nm, FESH0700, Thorlabs), and bandpass (400 ± 10 nm, Chroma Technology) filters.

Figure 1(b) depicts the acquisition procedure of the TM following an approach thoroughly described in Ref. [25]. The incident wave front is decomposed on the Hadamard basis—instead of the canonical basis—to benefit from higher fluence at the sample plane. For both linear- and nonlinear-feedback-based TM acquisition, the wave front phase of a Hadamard base for the incident field is shifted with respect to a reference field (the region in the periphery of the pattern shown in the SLM) in the range [0–2π] and the nonlinear (linear) intensity recorded by the emCCD (CMOS) camera, depending on the feedback scheme. After measuring all the Hadamard bases, a Fourier transform is applied on the scan of a single basis thus retrieving the phase of the nth basis with respect to the reference field. Once all the Hadamard bases are measured, a unitary transformation is applied to obtain the TM in the canonical basis [9,25]. Note that, in contrast with a monochromatic TM, the TM acquired here and used for optimization is measured under broadband conditions (see Appendix A). This might lead to quite different enhancement behaviors of the resulting focused beam depending on the scattering medium used, and on the optimization method used, as recently observed [17].

Two different schemes are used for inspection of the signal enhancements depending on the nature of the feedback used for acquiring the TM. In the nonlinear feedback scheme, the wave front necessary to enhance at a specified position is displayed on the SLM and the nonlinear image taken with the emCCD. In the linear feedback scheme, the retrieved TM contains the information necessary to spatially refocus in the region of interest (ROI) acquired. We then raster-scan the refocus using the different elements of the TM at each CMOS pixel within the ROI containing the nano-KTP. In parallel, we collect the

SHG signal integrated within the imaged plane by the PMT. A background subtraction was performed on the SHG images.

B. Samples

Two types of scattering media were used: a commercial diffuser (10° Light Shaping Diffuser, Newport) and a thin TiO_2 film (multiply-scattering medium). The TiO_2 film was fabricated by drop cast from a colloidal solution of amorphous 500-nm-diam TiO_2 plain particles dispersed in water (Corpuscular Inc.). The obtained thickness ($\approx$20 μm) is thicker than the l_t for this system (l_t for TiO_2 is expected to be a few micrometers) [18,26]. The collagen fibers were extracted from rat tail tendons as in Ref. [27] and placed between two coverslips separated by a 120-μm-thick spacer and filled with agarose solution. Nano-KTP crystals of 150 nm diameter are used to monitor the SHG enhancement obtained after both linear and nonlinear feedback. These nanocrystals are in particular of superior photostability [28] as compared to fluorescent samples that are likely to photobleach [15,29]. Quantitative analysis is based on single isolated nanocrystals in order to avoid any bias due to multiple interference sources, such as clustered particles.

III. RESULTS

A. Nonlinear enhancement from nonlinear feedback

In this section, we address the use of nonlinear feedback to obtain nonlinear enhancements. Quantifying performances in this regime can serve as reference values for later use on linear TM refocusing. Figure 2(a) shows SHG images obtained when a single isolated nano-KTP crystal is placed behind a diffuser, using nonoptimized and optimized wave fronts. The optimized image is formed after WS has been performed at

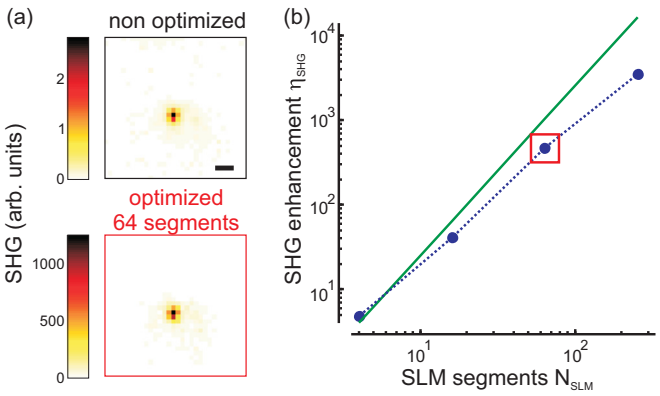

FIG. 2. Nonlinear signal enhancement based on a nonlinear feedback of a single 150-nm-diam nano-KTP crystal through a scattering medium (diffuser). (a) SHG wide field images, taken with the emCCD, before (top) and after WS (bottom). The nonoptimized image is an average over nonoptimal wave fronts, whereas the optimized image is a single frame. Scale bar: 1.6 μm. (b) SHG enhancement of a single particle versus the number of independently controlled SLM segments (blue markers, dashed line). The red box refers to the point depicted in (a). The continuous green line is a quadratic dependence of the nonlinear enhancement with respect to linear enhancements estimated after Ref. [9].

the nano-KTP position, exploiting the information obtained from the TM subelements measured using nonlinear photons at this specific position. This acquired row of the TM is the same as obtained in linear-feedback-based monochromatic TM as is widely used [9] (see Appendix A for further discussion on TMs). The approach evidences the capacity of the nonlinear-feedback-based TM to refocus light on a specific isolated nanocrystal and to generate a high nonlinear response.

Remarkably, nonlinear enhancements up to four orders of magnitude are achieved by using a few hundreds of independently controlled SLM segments (N_{SLM}). In order to quantify the gain in signal levels, we define the nonlinear enhancement η_{SHG} [13] as

$$\eta_{SHG} = \frac{I^{(2)}_{WS}}{\langle I^{(2)} \rangle},$$

where $I^{(2)}_{WS}$ and $I^{(2)}$ are SHG intensities at the particle position with optimized (WS) and nonoptimized wave fronts, respectively, and $\langle\,\rangle$ denotes average over different speckle realizations (here taken as a speckle generated by various Hadamard bases). Figure 2(b) shows that the nonlinear enhancement obtained from a single nano-KTP signal depends quadratically on N_{SLM} (the departure at high N_{SLM} is attributed to experimental artifacts such as possible correlations between SLM segments [25]). This expected dependence ascertains that the refocused spot preserves optimal nonlinear coherent buildup.

The nonlinear enhancements measured here are far above what has been previously reported in multiply-scattering media using even higher N_{SLM} values [13]. This difference is mainly assigned to the scattering regime used, for which speckle spectral correlation width is much lower than the spectral bandwidth of the source: $\Delta\lambda \ll \delta\lambda$. In other words, the pulse length of 130 fs surpasses the Thouless time of the medium, related to the width of the time of flight of photons propagating through the medium [30]. A simple and straightforward way to estimate the pulse lengthening is by measuring the speckle contrast [17,18,31]: for the scattering medium used a speckle contrast of 0.98 has been measured, which indeed fulfills the condition $\Delta\lambda \leqslant \delta\lambda$. Note that this lengthening scales as L^2/D [30], with D the diffusion constant of photons in the medium ($D = \frac{1}{3} v l_t$, v the energy velocity) and L the medium thickness [17,18].

Even though nonlinear feedback is able to provide remarkably high enhancements, it still imposes practical constraints. Using 64 controllable SLM segments requires in particular TM acquisition times of the order of minutes, which can be at an extreme cost for nonlinear imaging. Furthermore, this methodology also relies on low signals, especially at large depths, and can be only measured in regions where nonlinear signal is emitted. To answer these issues, we address in the next section the use of the overwhelming linearly scattered photons for nonlinear signal enhancements.

B. Nonlinear enhancement from linear TM refocusing

The principle of SHG image reconstruction by linear feedback is sketched in Fig. 3(a). After acquiring the linear TM of the system, refocus is formed at a desired location, with simultaneous acquisition of nonlinear signals, resembling

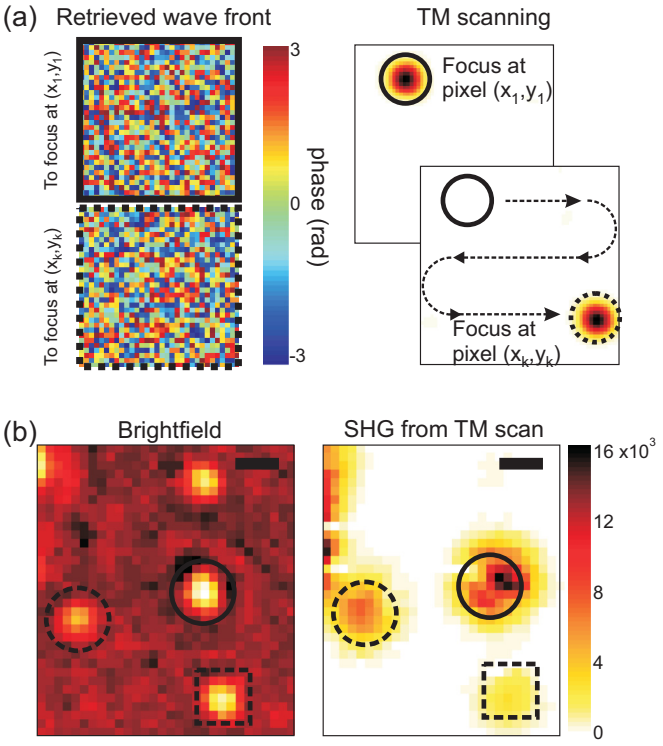

FIG. 3. Nonlinear signal enhancement based on a linear feedback through a scattering medium (diffuser). (a) After acquisition of the linear TM, wave fronts are tailored to refocus the beam at desired positions through the scattering medium. The optimal wave fronts obtained for two different refocus positions (right) are shown (left). The SHG image is formed by a raster scanning of the refocus positions obtained from the linear-feedback-based TM, and acquisition of the SHG signal simultaneously. (b) Comparison between a bright field image (left) and the obtained corresponding SHG image (right). Number of controlled SLM segments: 2^{12}. Scale bar: 0.9 μm.

raster-scanning methodologies. Alternatively, one could use the angular memory effect to raster-scan the refocus and obtain the final SHG image, with a field of view that depends on the scattering medium properties [15,32–34]. Figure 3(a) shows representative incident wave fronts corresponding to the two positions of the refocus, showing no correlation as expected in multiple-scattering conditions. To validate the imaging mode methodology for nonlinear optics, we compare in Fig. 3(b) the SHG image of isolated nano-KTP crystals acquired by refocus scanning, with a bright field image taken without the scattering medium. The positions of the three detected nanocrystals are in excellent agreement with the bright field image. The difference in SHG signal levels is due to the relative orientation of the crystal with respect to the polarization state of the excitation field, indicating that the polarization of the refocused beam might also be conserved [35–39].

Figure 4 summarizes the imaging enhancement performances evaluated on single nano-KTP crystals, for various N_{SLM} values after two scattering media: a surface diffuser and a multiply scattering medium with a thickness of a few l_t's. Linear enhancements (η) are defined as

$$\eta = \frac{I_{WS}}{\langle I \rangle},$$

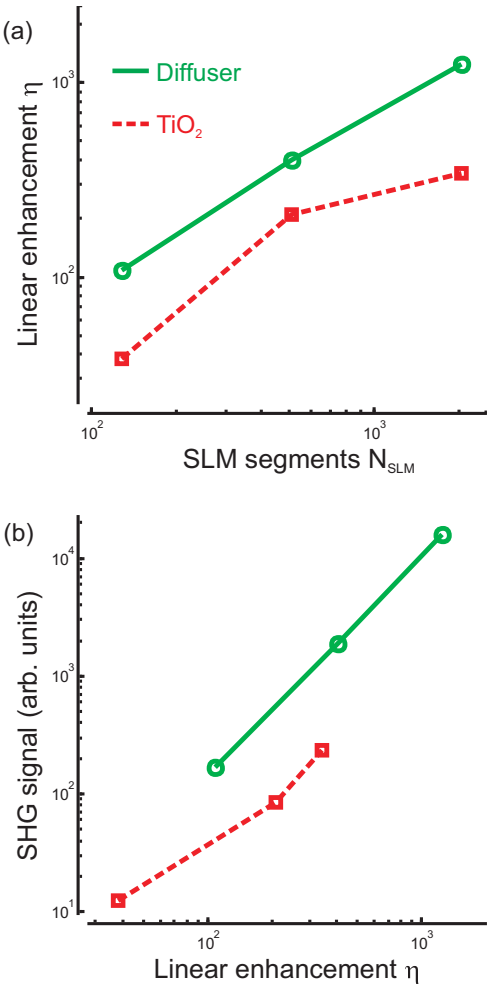

FIG. 4. Linear refocusing and nonlinear efficiencies obtained after linear feedback in two different scattering media, diffuser and 20-μm-thick TiO_2 film. (a) Linear enhancement obtained as a function of the numbers of SLM segments, N_{SLM}. (b) SHG signal dependence on the linear enhancement.

where I_{WS} is the intensity at the refocus position with optimal wave front (WS) and $\langle I \rangle$ the averaged intensity obtained under nonoptimal wave fronts. SHG signals are averaged over several nano-KTPs, circumventing the bias due to orientational effects. While the diffuser system fulfills $\Delta\lambda \leqslant \delta\lambda$, the 20-$\mu$m-thick TiO_2 film departs from this situation and exhibits a speckle contrast of 0.59, corresponding to a broadening of the pulse by approximately threefold [17,31]. As a consequence, the linear enhancement values [Fig. 4(a)] are seen to be higher for the diffuser than the TiO_2 film, which is expected from the higher number of spectral modes excited for the latter [7,17]. Under broadband refocusing conditions, the loss in linear enhancement between the two considered media is expected to be about a factor of 2 considering the measured speckle contrasts [17], which is close to what is measured here at a relatively low number of segments N_{SLM} (high N_{SLM} values are more sensitive to possible artifacts).

Figure 4(b) shows nonlinear efficiencies generated after refocusing on nano-KTPs in both scattering media. In order to correct for systematic linear enhancement drift at high

N_{SLM} values, we plot the SHG signal versus the linear focus enhancement η. Both media exhibit an almost quadratic dependence of the SHG signal with η, evidencing the capabilities of the linear optimization scheme to preserve the nonlinear coupling quality whatever the number of SLM segments used. Importantly in the case of the diffuser, the SHG *enhancements* η_{SHG} are the same as that obtained in the nonlinear feedback process described above (data not shown). However, the signals obtained through TiO_2 are an order of magnitude lower than for the diffuser (SHG enhancements could not be quantified for TiO_2 due to the low signal-to-noise ratio before optimization). This is visibly a consequence of smaller $\delta\lambda$ of the TiO_2 film, which is likely to lead to pulse lengthening and thus to lower nonlinear coupling efficiency. SHG signals (after WS) are nevertheless of high signal-to-noise ratio and evidence the remarkable capacity of broadband linear refocusing through scattering media to produce efficient nonlinear conversion. This emphasizes that in conditions where medium and laser spectral bandwidth are of similar magnitude, both methodologies lead to efficient spatiotemporal coupling effects, most probably preserving short pulse width after refocusing.

At last, the acquisition of the TM for $N_{SLM} = 256$ takes about 40 s, which is considerably faster than in the nonlinear feedback procedure (30 min) under the same conditions. As a matter of fact, a linear feedback is typically limited by the SLM speed, which can reach millisecond refocusing rates, rather than signal-to-noise issues as in a nonlinear feedback scheme.

C. Nonlinear bioimaging behind a thick scattering medium

We finally apply the linear feedback TM measurement to nonlinear imaging in a biological SHG-active thick sample, made of collagen fibers extracted from rat tail tendons (thickness 120 μm), a widely studied specimen in SHG microscopy [40,41]. Figure 5 shows an SHG image of such a sample placed behind a diffuser, acquired after the TM has been measured. To obtain the final SHG image, we first acquired a linear optical image that is used for normalization, allowing correction for possibly remaining spatially nonuniform refocus [42] (see Appendix B).

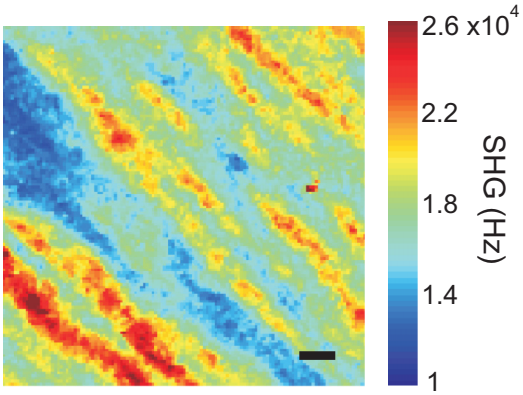

FIG. 5. SHG imaging of rat tail tendon collagen. Scattering medium: diffuser. Number of controlled SLM segments: 2^{10}. Scale bar: 2.3 μm.

Thick fibers are visible along the diagonal of the image, with a high SHG signal that is clearly above the background signal level. Without WS, a raster scanning (mimicking a conventional nonlinear microscopy experiment) of the focus did not generate a discernible image of the collagen fibers but only a noisy unresolved image arising from the speckle excitation. The obtained image is also a remarkable improvement as compared to the use of nonlinear feedback optimization, which not only gave lower SHG enhancements (four times lower η_{SHG}) but mostly suffers from considerably slower optimization speeds (ten times slower). This nonlinear sample indeed differs strongly from nano-KTPs since its response is much less sparse: in this regime, the presence of background nonlinear signals from the sample volume and surface is likely to make the nonlinear optimization process biased and much less efficient [19,20].

IV. DISCUSSION

This study shows that the medium speckle spectral correlation width $\delta\lambda$ is a key factor for the manipulation of the broadband TM in scattering media, as already evidenced in the monochromatic regime in multiple-scattering media at a few l_t's [18]. We have demonstrated that in the regime $\delta\lambda \approx \Delta\lambda$, both linear and nonlinear feedback acquisition of the TM lead to comparable nonlinear enhancements. This last condition is typically met at 1 mm thickness or depth in biological systems at 800-nm wavelengths [21]. Beyond such depth in anisotropic scattering media, as in biological tissues [43], the fluence is expected to decrease, thus becoming the limiting factor for nonlinear excitation. However, one could forecast the possibility to generate nonlinear signals using higher energy-per-pulse lasers at a reduced repetition rate [20].

Our results show that refocusing through a scattering medium using the linear TM can allow faster and more efficient nonlinear imaging. Other advantages of the use of linear feedback can be highlighted. First, nonlinear feedback requires fluorescent [14,15] or SHG [13] active guide stars. Under low signal-to-noise conditions, the feedback mechanism might thus fail or lead to large optimization times. Second, nonlinear feedback is inherent to the nonlinear mechanism used for the optimization procedure. Spatial and temporal properties of the refocus depend on the size of the nonlinear effective volume, on the nonlinear order (two-photon, three-photon, etc.) of the process used, and on its coherence (SHG versus two photon fluorescence, for instance; coherent nonlinear effects indeed involve phase-matching conditions that might depend on the object size). Optimization for a given nonlinear process is therefore not necessarily appropriate for other nonlinear processes and samples. Third, the presence of sparse bright regions in the sample can bias the optimization conditions if a large dynamic range of signals is present in the sample [15].

We anticipate that a linear feedback in hybrid approaches may enable superpenetration of NLM. Considerable advances have been made recently towards the direction of linear refocusing *inside* scattering media. In particular, acousto-optic [44–46] or photoacoustic [10,47–49] guide stars have been developed to take advantage of the ballistic penetration

of acoustic waves in biological tissues. The use of photoacoustic time traces to monitor the TM inside the medium could for instance be advantageously coupled to nonlinear detection, in both backward and forward directions. Other recent demonstrations using the intrinsic dynamic fluctuations of the speckle pattern [22,23], assisted by digital optical phase conjugation to refocus, could be also combined with NLM with the benefit of achieving speckle-size refocus. In a more realistic scenario, recent applications of wave front shaping for optical coherence tomography have demonstrated enhanced penetration depth [24], with the latter being conveniently coupled with NLM [50–52], thus highlighting that addressing linear feedback can be considerably more advantageous.

Regarding the raster-scanning modality presented in Sec. III B, we believe that a hybrid methodology may have even faster imaging capability. Although we measured an oversampled TM to image in a raster-scanning fashion, one could measure a TM with undersampled output modes and use the translational memory effect [53] to locally scan the refocus [39]. This hybrid approach has the advantage of a much wider field of view than accessible by the translational memory effect.

At last, the expected large $\delta\lambda$ of biological media at millimeter depth opens interesting prospectives for multicolor nonlinear microscopy, such as multilabel fluorescence or coherent Raman (CR) imaging. In CR microscopy if the vibrational resonance lies within the spectral width of the medium, only a single wavelength would be necessary to characterize the TM of the system. Such a situation may be found at 0.1–0.2 l_t depths at which CR microscopy has not yet been able to image [54,55]. Our observations also suggests that for higher-order (>2) processes, e.g., three-photon fluorescence, third-harmonic generation, or coherent anti-Stokes Raman scattering, enhancements above three orders of magnitude could be generated by using cheaper low-resolution SLMs. Because in the present method we are addressing the linearly scattered photons, our conclusions are valid for any nonlinear contrast imaging modality.

V. CONCLUSIONS

We have compared different feedback mechanisms for acquiring the TM of the scattering system and thus enhancing nonlinear signals, using as a model system SHG from nano-KTP and collagen fibers. If the medium speckle spectral correlation width $\delta\lambda$ is much larger than the excitation source $\Delta\lambda$, i.e., in the regime where the pulse is not temporally broadened, both feedback mechanisms lead to the same nonlinear enhancement. However, under certain situations, such as the presence of a high nonlinear background, a linear feedback leads to a much faster and stronger enhancement. In the regime where the pulse is broadened by the medium, while nonlinear methods suffer from low initial nonlinear signal, our approach still works and allows significant speedup. The conclusions drawn are particularly useful for imaging biological systems at millimeter depth where $\delta\lambda$ is comparable with $\Delta\lambda$ and the low number of nonlinear photons may be the difficulty. We ended by extensively discussing the possibility of combining a linear TM approach with current methods which refocus inside the medium for prospective deep nonlinear imaging.

ACKNOWLEDGMENTS

We thank Esben Andressen and Herve Rigneault for initial tests on their setup and fruitful discussions, Ori Katz for technical assistance, Thierry Gacoin and Ludovic Meyer for providing the nano-KTP particles, and Yannick Foucault for characterizing the TiO_2 films. H.B.A. thanks the FEMTO network of Mission pour l'Interdisciplinarité (CNRS, France) for its financial support. This work was supported by Agence Nationale de la Recherche (ANR) under Contracts No. ANR-10-INBS-04-01 (France-BioImaging infrastructure network), No. ANR-11-INSB-0006 (France Life Imaging infrastructure network), and No. ANR-15-CE19-0018-01(MyDeepCARS), and European Research Council (ERC) (Grant No. 278025).

APPENDIX A: DISCUSSION ON THE TM ACQUIRED

The linear TM of the medium is measured under (spectrally) broadband conditions: the measured interferometric modulation is the spectrally integrated modulation measured on the detector. For a medium with negligible lengthening, this approach is equivalent to Ref. [9], whereas for a medium that lengthens the pulse, the acquired TM can be seen as the incoherent sum of different spectral contributions. In the linear and monochromatic case, an output mode $E_m^{(o)}$ is related to an input mode $E_n^{(i)}$ through the transmission-matrix elements t_{mn},

$$E_m^{(o)} = \sum_n t_{mn} E_n^{(i)},$$

$$\mathbf{E}^{(o)} = \mathbf{t}\mathbf{E}^{(i)}.$$

In general, $\mathbf{t}$ for scattering media has a dependence on wavelength [18] and polarization states combinations [39]. However, when correlations of polarization states exist [39] and the pulse is not lengthened [14] (for instance, in thin scattering media), the TM measured with a nonlinear feedback does reflect the linear TM. This is so because the SHG process involving a strong reference field and a weak modulated field leads to an interference pattern dominated by their relative phase (not by its higher harmonics) [13], hence behaving similarly as for a monochromatic TM measurement [25]. Obviously, a thin and spatially homogeneous nonlinear active sample would be required to determine the full TM of the scattering medium, similarly as in linear optics. As a matter of fact, we have experimentally tested and both methods are equivalent; that is, a linear-feedback-based TM does refocus SHG light, and a nonlinear-feedback-based TM does refocus linear light.

APPENDIX B: NORMALIZATION PROCEDURE

In this section, we describe the normalization procedure used for generating Fig. 5. When acquiring a TM, one needs to use a reference field. In our scheme, the reference field is a non-wave front-shaped speckle originating from the periphery of the focusing lens. In turn, there will be regions (in the field of view) where the reference speckle has intensity that is below the noise level, thus leading to inaccurate retrieval of

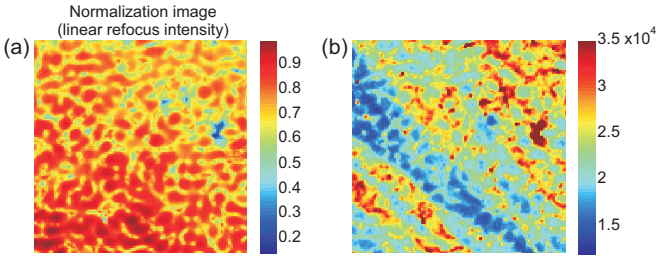

FIG. 6. (a) Relative intensity of the refocus in the field of view presented in Fig. 5. This image is a normalization image to correct for a nonuniform refocus in the field of view. (b) Because of the strong SHG background level arising from a nonsparse sample, normalization of the raw SHG signal by the squared normalization image leads to a noisier image.

TM elements and therefore lower enhancement values [42]. Because of the nonlinear dependence of the SHG signal on the refocus intensity [Fig. 2(b)], we first acquired the linear refocus intensity to build an image for normalization of the SHG signal. This normalization image is presented in Fig. 6(a).

The image presented in Fig. 5 is normalized by dividing the raw SHG data by the normalization image using an adaptive method. Because of the high background (originating from the volume excited by the speckle background), a conventional normalization by this squared normalization image leads to a noisier SHG image as shown in Fig. 6(b). Therefore, we implemented an adaptive model that finds the smoothest image. We calculated the spatially averaged contrast of the image $I_{\mathrm{SHG}}/I_{\mathrm{ref}}^{\kappa}$—where I_{SHG} is the background-subtracted SHG image, I_{ref} is the linear normalization image, and κ is a number fixed within the same normalization image—in order to find κ which leads to the lowest contrast, that is, to a smooth image. For the image shown in Fig. 5, $\kappa = 1.6$ (we have added the background to stress its presence). We have simulated this situation numerically, and corroborated experimentally with a homogeneous solution using a two-photon excited fluorescence process (data not shown), and found out that the precise value of κ will strongly depend on the level of background signal with respect to the signal originating from the refocus position.

This outcome further highlights the importance of obtaining nonlinear enhancements close to theoretical values when the nonlinear signal is nonsparse. Since the methodology used is out of scope of the present study, we are currently evaluating how this effect would impact various other nonlinear optical processes depending on the sample sparsity level. Note that a sparse sample, such as presented in Fig. 1, does not present this issue.

[1] J. Mertz, *Introduction to Optical Microscopy* (Roberts and Company, Greenwood Village, 2010).
[2] F. S. Pavone and P. J. Campagnola, *Second Harmonic Generation Imaging* (CRC Press, Boca Raton, FL, 2013).
[3] D. Débarre, E. J. Botcherby, T. Watanabe, S. Srinivas, M. J. Booth, and T. Wilson, Opt. Lett. **34**, 2495 (2009).
[4] J. Tang, R. N. Germain, and M. Cui, Proc. Natl. Acad. Sci. USA **109**, 8434 (2012).
[5] C. Wang, R. Liu, D. E. Milkie, W. Sun, Z. Tan, A. Kerlin, T.-W. Chen, D. S. Kim, and N. Ji, Nat. Meth. **11**, 1037 (2014).
[6] D. Sinefeld, H. P. Paudel, D. G. Ouzounov, T. G. Bifano, and C. Xu, Opt. Express **23**, 31472 (2015).
[7] A. P. Mosk, A. Lagendijk, G. Lerosey, and M. Fink, Nat. Photon. **6**, 283 (2012).
[8] I. M. Vellekoop and A. P. Mosk, Opt. Lett. **32**, 2309 (2007).
[9] S. M. Popoff, G. Lerosey, R. Carminati, M. Fink, A. C. Boccara, and S. Gigan, Phys. Rev. Lett. **104**, 100601 (2010).
[10] T. Chaigne, O. Katz, A. Boccara, M. Fink, E. Bossy, and S. Gigan, Nat. Photon. **8**, 58 (2013).
[11] D. Akbulut, T. Huisman, E. van Putten, W. Vos, and A. P. Mosk, Opt. Express **19**, 4017 (2011).
[12] D. B. Conkey, A. M. Caravaca-Aguirre, and R. Piestun, Opt. Express **20**, 1733 (2012).
[13] J. Aulbach, B. Gjonaj, P. Johnson, and A. Lagendijk, Opt. Express **20**, 29237 (2012).
[14] O. Katz, E. Small, Y. Bromberg, and Y. Silberberg, Nat. Photon. **5**, 372 (2011).
[15] O. Katz, E. Small, Y. Guan, and Y. Silberberg, Optica **1**, 170 (2014).
[16] I. M. Vellekoop, Opt. Express **23**, 12189 (2015).
[17] H. P. Paudel, C. Stockbridge, J. Mertz, and T. Bifano, Opt. Express **21**, 17299 (2013).
[18] D. Andreoli, G. Volpe, S. Popoff, O. Katz, S. Gresillon, and S. Gigan, Sci. Rep. **5**, 10347 (2015).
[19] P. Theer and W. Denk, J. Opt. Soc. Am. A **23**, 3139 (2006).
[20] N. G. Horton, K. Wang, D. Kobat, C. G. Clark, F. W. Wise, C. B. Schaffer, and C. Xu, Nat. Photon. **7**, 205 (2013).
[21] O. Katz, P. Heidmann, M. Fink, and S. Gigan, Nat. Photon. **8**, 784 (2014).
[22] E. H. Zhou, H. Ruan, C. Yang, and B. Judkewitz, Optica **1**, 227 (2014).
[23] C. Ma, X. Xu, Y. Liu, and L. V. Wang, Nat. Photon. **8**, 931 (2014).
[24] J. Jang, J. Lim, H. Yu, H. Choi, J. Ha, J.-H. Park, W.-Y. Oh, W. Jang, S. Lee, and Y. Park, Opt. Express **21**, 2890 (2013).
[25] S. M. Popoff, G. Lerosey, M. Fink, A. C. Boccara, and S. Gigan, New J. Phys. **13**, 123021 (2011).
[26] J. Aulbach, B. Gjonaj, P. M. Johnson, A. P. Mosk, and A. Lagendijk, Phys. Rev. Lett. **106**, 103901 (2011).
[27] D. Aït-Belkacem, A. Gasecka, F. Munhoz, S. Brustlein, and S. Brasselet, Opt. Express **18**, 14859 (2010).
[28] L. Le Xuan, C. Zhou, A. Slablab, D. Chauvat, C. Tard, S. Perruchas, T. Gacoin, P. Villeval, and J.-F. Roch, Small **4**, 1332 (2008).
[29] I. M. Vellekoop, E. G. van Putten, A. Lagendijk, and A. P. Mosk, Opt. Express **16**, 67 (2008).
[30] A. Z. Genack and J. M. Drake, Europhys. Lett. **11**, 331 (1990).
[31] N. Curry, P. Bondareff, M. Leclercq, N. F. van Hulst, R. Sapienza, S. Gigan, and S. Grésillon, Opt. Lett. **36**, 3332 (2011).
[32] I. M. Vellekoop and C. M. Aegerter, Opt. Lett. **35**, 1245 (2010).
[33] G. Ghielmetti and C. M. Aegerter, Opt. Express **22**, 1981 (2014).
[34] S. Schott, J. Bertolotti, J.-F. L. ger, L. Bourdieu, and S. Gigan, Opt. Express **23**, 13505 (2015).

[35] D. Bicout, C. Brosseau, A. S. Martinez, and J. M. Schmitt, Phys. Rev. E **49**, 1767 (1994).
[36] M. Xu and R. R. Alfano, Phys. Rev. Lett. **95**, 213901 (2005).
[37] N. Ghosh, H. Patel, and P. Gupta, Opt. Express **11**, 2198 (2003).
[38] H. B. de Aguiar, P. Gasecka, and S. Brasselet, Opt. Express **23**, 8960 (2015).
[39] H. B. de Aguiar, S. Gigan, and S. Brasselet, arXiv:1511.02347.
[40] S. Roth and I. Freund, J. Chem. Phys. **70**, 1637 (1979).
[41] S. Bancelin, C. Aimé, I. Gusachenko, L. Kowalczuk, G. Latour, T. Coradin, and M.-C. Schanne-Klein, Nat. Commun. **5**, 4920 (2014).
[42] X. Tao, D. Bodington, M. Reinig, and J. Kubby, Opt. Express **23**, 14168 (2015).
[43] W. Cheong, S. Prahl, and A. Welch, IEEE J. Quantum Electron. **26**, 2166 (1990).
[44] X. Xu, H. Liu, and L. V. Wang, Nat. Photon. **5**, 154 (2011).
[45] Y. M. Wang, B. Judkewitz, C. A. DiMarzio, and C. Yang, Nat. Commun. **3**, 928 (2012).
[46] B. Judkewitz, Y. M. Wang, R. Horstmeyer, A. Mathy, and C. Yang, Nat. Photon. **7**, 300 (2013).
[47] F. Kong, R. H. Silverman, L. Liu, P. V. Chitnis, K. K. Lee, and Y.-C. Chen, Opt. Lett. **36**, 2053 (2011).
[48] D. B. Conkey, A. M. Caravaca-Aguirre, J. D. Dove, H. Ju, T. W. Murray, and R. Piestun, Nat. Commun. **6**, 7902 (2015).
[49] P. Lai, L. Wang, J. W. Tay, and L. V. Wang, Nat. Photon. **9**, 126 (2015).
[50] E. Beaurepaire, L. Moreaux, F. Amblard, and J. Mertz, Opt. Lett. **24**, 969 (1999).
[51] J. S. Bredfeldt, C. Vinegoni, D. L. Marks, and S. A. Boppart, Opt. Lett. **30**, 495 (2005).
[52] T. Kamali, B. Považay, S. Kumar, Y. Silberberg, B. Hermann, R. Werkmeister, W. Drexler, and A. Unterhuber, Opt. Lett. **39**, 5709 (2014).
[53] B. Judkewitz, R. Horstmeyer, I. M. Vellekoop, I. N. Papadopoulos, and C. Yang, Nat. Phys. **11**, 684 (2015).
[54] A. J. Wright, S. P. Poland, J. M. Girkin, C. W. Freudiger, C. L. Evans, and X. S. Xie, Opt. Express **15**, 18209 (2007).
[55] A. Taruttis and V. Ntziachristos, Nat. Photon. **9**, 219 (2015).